Acoustic waves generated by a laser line pulse in cylinders; Application to the elastic constants measurement

Y. Pan[a)]
Institute of Acoustics, Tongji University, 200092, Shanghai, People's Republic of China

C. Rossignol and B. Audoin
Laboratoire de Mécanique Physique, UMR CNRS 8469, Université Bordeaux 1, 33405 Talence, France

(Received 5 August 2003; revised 8 January 2004; accepted 9 January 2004)

A model is proposed to predict acoustic waves generated in a transversely isotropic cylinder by a laser line pulse extended in beamwidth and time duration, and an application to elastic constants measurement is presented. Documented good agreements are observed in the comparison of experimental and theoretical normal displacements for aluminum cylinders under either ablation or thermoelastic generation. Bulk waves are identified and processed for the elastic constants measurement. The effects of source beamwidth and time duration on wave forms and on the elastic constants measurement are predicted by numerical simulations. For nondestructive evaluation applications using bulk waves, a radius of 0.3 mm appears as a minimum limit for the sample size using a laser source of 0.1 mm beamwidth and 20 ns time duration. Elastic constants of aluminum rods are experimentally measured with very good accuracy. © *2004 Acoustical Society of America.* [DOI: 10.1121/1.1651191]

PACS numbers: 43.35.Cg, 43.35.Zc, 43.20.Bi. [YHB] Pages: 1537–1545

I. INTRODUCTION

Cylindrical parts often acting as rotating axes of a machine play important roles. Nowadays, they are in a particular favor of new materials with enhanced mechanical properties such as fiber-enhanced composite materials, which have high performance in strength and durability. Many manufactured rods, fibers, and other cylindrical structures have transverse isotropy. There is an increasing demand of measuring nondestructively their elastic constants, which are often directly related to their mechanical performances. Additionally, a cylinder with its unique geometry is a basic target for the acoustic wave propagation research.

Understanding the wave propagation in a cylinder is a necessary step before considering any possible application. Surface acoustic or Rayleigh wave propagating on an isotropic and homogeneous cylinder was considered in 1927 by Sezawa,[1] who obtained its characteristic equation and calculated the dependence of its velocity on the radius of the cylinder. More detailed studies were reported in 1967 by Viktorov,[2] who calculated its dispersive curve and made a comparison to experimental data detected by conventional piezoelectric transducers. Higher Rayleigh-type waves were termed as "Whispering-gallery modes" by Uberall in 1973.[3] Due to the coupling difficulty of such transducers, few experimental reports on the wave propagation for a curved medium had been published until the development of the laser ultrasonic technique,[4] in which ultrasonic waves are both generated and detected by lasers. With the remarkable features of noncontact, high spatial and temporal resolutions introduced by this technique, various studies on materials of curved surfaces have been carried out. As an example, Rayleigh wave propagating on a sphere was observed experimentally in 1988,[5] and a further detailed study has been reported later.[6] Rayleigh wave propagating on a cylinder was also studied by this technique.[7,8] The finite element method has been used to predict the bulk and surface wave propagations when laser beam was focused by a cylindrical lens.[9] Very recently, authors have published a model[10] to successfully predict the bulk and surface wave propagations in a transversely isotropic cylinder under either ablation or thermoelastic generation. In this model, the laser pulse was represented by a sudden normal force with delta function in time for ablation generation or by a dipolar force with a Heavside step function in time for thermoelastic generation.[10] Since laser pulses have certain beamwidth and time duration, these representations can only hold true when the cylinder is large enough to neglect the influence of these physical dimensions. Therefore, it is necessary to take account of the influence when the radius of the cylinder turns to small values.

There has been considerable study of the acoustic scattering characteristics of a transversely isotropic cylinder for the purpose of determining its elastic properties. For a typical example, resonance acoustic spectroscopy, the study of resonance effects present in acoustic echoes of an elastic target, was proposed to evaluate the elastic constants of the cylindrical samples.[11] For this technique, the sample must be immersed in a fluid like water or another material. This limits its capability when the sample is not allowed to do so, such as the measurement at elevated temperatures. Actually, many new materials are intended for use at a high temperature. Another resonance technique, the measurement of longitudinal and torsional resonance frequencies of samples of known geometry, has determined nondestructively the elastic constants of various crystals at high temperature.[12] Free vibrations of a transversely isotropic finite cylindrical rod has been analyzed for the purpose of elastic constants

[a)]Electronic mail: y.pan@lmp.u-bordeaux1.fr

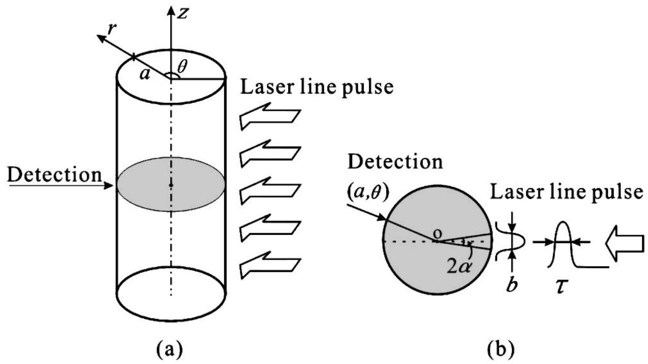

FIG. 1. Problem geometry.

determination.[13] But this technique requires proper machining of samples and fine identification of the resonance peaks. Moreover, noncontact measurement is not possible with this technique. Fortunately, the above limitations are circumvent with the laser ultrasonic technique, in which the ultrasonic waves are generated and detected at a distance, without any contact to the sample.

Recently, many studies have focused on applications of the surface acoustic waves by the laser ultrasonic technique. The velocities of the Rayleigh wave of steel rods receiving different heat treatments were measured to characterize the surface residual stress of the cylindrical parts.[14] The acoustic waves propagation in a sphere has been analyzed to establish a guideline for the design of a ball surface acoustic wave device.[6] The surface wave propagation on a cylinder has been studied to detect surface break defects.[15] According to the author's knowledge, no study on applications of bulk waves in either the sphere or cylinder has been reported using this technique.

In order to address cylinders of all possible sizes for both forward and inverse problems, the published model[10] is generalized in this paper to predict the acoustic waves generated in a transversely isotropic cylinder by a laser line pulse extended in beamwidth and time duration. The application to the measurement of the elastic constants is further considered. At first, the general problem is formulated in Sec. II. Transformed solutions of the generalized model and an inverse transform scheme are presented in Sec. III. To validate the modeling, the calculated normal displacements of aluminum cylinders under either ablation or thermoelastic generation are compared to the experimental signals detected by the laser ultrasonic technique, in Sec. IV. The effects of the source beamwidth and time duration are fully analyzed in Sec. V. Finally, the elastic constants measured on both calculated and experimental wave forms under either generation regime are presented and discussed in Sec. VI.

II. GENERAL FORMULATION

Let us consider a homogeneous and transversely isotropic cylinder of infinite length, radius a, and density ρ. As shown in Fig. 1(a), the symmetrical axis of the cylinder is assumed to coincide with the z axis of its cylindrical coordinates $(r,\ \theta,\ z)$. A pulsed laser is used to generate acoustic waves in this material. Here, "detection" is to denote an experimental technique, generally an optical detection technique,[4] which is applied to measure these acoustic waves. If a cylindrical lens is used to focus the laser beam, this laser can be modeled as a line-like acoustic source, which lies at the boundary of the cylinder, $r=a$, and extends along the z direction. As shown in Fig. 1(b), the laser source is assumed to have a beamwidth b and a time duration τ, and it impacts on the cylindrical surface of an area with a cylindrical angle 2α. To denote the detection position on the cylinder, cylindrical coordinates $(a,\ \theta)$ are chosen, considering $\theta=0$ for the source position.

Let c_{11} and c_{12} denote the two independent elastic constants related to the isotropic plane perpendicular to the z axis. Owing to the symmetry imposed by the source shape, this problem shows invariance along the z direction. The nonzero components of the displacement vector depend on two spatial variables r, θ and on time t. These components, denoted u_r and u_θ can be written as[16]

$$u_r(r,\theta,t)=\frac{\partial\varphi}{\partial r}+\frac{1}{r}\frac{\partial\chi}{\partial\theta},$$
$$u_\theta(r,\theta,t)=\frac{1}{r}\frac{\partial\varphi}{\partial\theta}-\frac{\partial\chi}{\partial r}, \tag{1}$$

where the two scalar potentials φ and χ are governed by the following wave motion equations:

$$\frac{\partial^2\varphi}{\partial r^2}+\frac{1}{r}\frac{\partial\varphi}{\partial r}+\frac{1}{r^2}\frac{\partial^2\varphi}{\partial\theta^2}=\frac{\rho}{c_{11}}\frac{\partial^2\varphi}{\partial t^2},$$
$$\frac{\partial^2\chi}{\partial r^2}+\frac{1}{r}\frac{\partial\chi}{\partial r}+\frac{1}{r^2}\frac{\partial^2\chi}{\partial\theta^2}=\frac{2\rho}{(c_{11}-c_{12})}\frac{\partial^2\chi}{\partial t^2}. \tag{2}$$

Before turning our attention to the boundary conditions, let us define $q(t)$ as the normalized function that represents the source time dependency. Normalization means that the integral of $q(t)$ over its variable equals unity. This function is chosen for the pulsed laser source with a rise time $\tau/2$, i.e., pulse duration τ as[17]

$$q(t)=\frac{4t}{\tau^2}e^{-2t/\tau},\quad \text{for}\ \ t\geqslant 0. \tag{3}$$

In the remainder, $q(t)$ will be changed in to the delta function $\delta(t)$ when a source duration $\tau=0$ is considered. Reciprocally, in the space domain, since ablation occurs when the density of the laser light intensity overpasses a certain threshold,[18] the acoustic source distribution is considered as

$$g_A(\theta)=\begin{cases}\dfrac{1}{2\alpha}, & -\alpha\leqslant\theta\leqslant\alpha,\\[2mm] 0, & \text{other,}\end{cases} \tag{4}$$

for this generation. Additionally, the distribution for the thermoelastic generation is assumed to be proportional to the light intensity.[19] Therefore a normalized Gaussian function,

$$g_T(\theta)=\frac{1}{2\alpha\sqrt{\pi}}e^{\frac{-\vartheta^2}{4\alpha^2}}, \tag{5}$$

represents the acoustic source in this generation. In Eqs. (4)–(5), the angle α is determined by the beamwidth and the cylindrical radius as $\alpha=\arctan(b/a)$; see Fig. 1(b). Here $g_T(\theta)$

and $g_A(\theta)$ will be changed into the delta function $\delta(\theta)$ when a source width $b=0$ is considered.

Then, two components σ_{rr} and $\sigma_{r\theta}$ of the stress tensor at any point of the surface must comply with the following boundary conditions:

$$\begin{cases} \sigma_{rr}|_{r=a} = -F_0 f(t) \sum_{n=-\infty}^{+\infty} g_A(\theta - 2n\pi), \\ \sigma_{r\theta}|_{r=a} = 0, \end{cases} \tag{6}$$

for the ablation generation,[18] or

$$\begin{cases} \sigma_{rr}|_{r=a} = 0, \\ \sigma_{r\theta}|_{r=a} = -F_0 \int_0^t f(\varepsilon) d\varepsilon \sum_{n=-\infty}^{+\infty} \frac{\partial g_T(\theta - 2n\pi)}{\partial \theta}, \end{cases} \tag{7}$$

for the thermoelastic generation.[17] In Eqs. (6) and (7), F_0 is a certain loading in N.μs.m^{-1} related to the laser line pulse, and n stands for the number of clockwise ($n>0$) or counter-clockwise ($n<0$) roundtrips of the generated acoustic waves. Let us underline that adopting these expressions, a normal loading is considered in the ablation generation, Eq. (6), and a dipolar force is represented in Eq. (7) for the source shape in the thermoelastic generation.[20] Additionally, if the pulse duration is $\tau=0$, the ablative source is impulsive, and it shows a step-like evolution in the time domain for the thermoelastic generation since thermal diffusion is neglected.

III. TRANSFORMED SOLUTIONS AND NUMERICAL INVERSE SCHEME

The two-dimensional Fourier transform of the displacement field over the coordinate θ and time t is now considered, and it is noted as U_i ($i=r$ or θ). On noting $\nu = k_\theta a$, where k_θ is the component of the wave vector $\mathbf{k}$ along the θ direction, the nonzero components of the displacement at a given position and time are then as follows:

$$u_i(r,\theta,t) = \frac{1}{4\pi^2} \int \int_{-\infty}^{+\infty} U_i(r,\nu,\omega) e^{-j(\nu\theta - \omega t)} d\nu\, d\omega. \tag{8}$$

Doing so, the wave motion equations and the boundary equations can be linearized, providing explicit forms for the potentials φ and χ under either generation regime. Components of the displacement are then obtained for ablation generation,

$$U_r(r,\nu,\omega) = -\frac{F_0 a}{(c_{11}-c_{12})D_\nu} \frac{\mathrm{sinc}(\nu\alpha)}{(1+j\omega\tau)^2} \times \left\{ \left(\nu^2 - \frac{k_T^2 a^2}{2} - B_T \right) B_L \frac{J'_\nu(k_L r)}{J'_\nu(k_L a)} + \nu^2 (1-B_L) \frac{a}{r} \frac{J_\nu(k_T r)}{J_\nu(k_T a)} \right\} \sum_{n=-\infty}^{+\infty} e^{j\nu 2n\pi},$$

$$U_\theta(r,\nu,\omega) = \frac{j\nu F_0 a}{(c_{11}-c_{12})D_\nu} \frac{\mathrm{sinc}(\nu\alpha)}{(1+j\omega\tau)^2} \times \left\{ \left(\nu^2 - \frac{k_T^2 a^2}{2} - B_T \right) \frac{a}{r} \frac{J_\nu(k_L r)}{J_\nu(k_L a)} + (1-B_L) B_T \frac{J'_\nu(k_T r)}{J'_\nu(k_T a)} \right\} \sum_{n=-\infty}^{+\infty} e^{j\nu 2n\pi}, \tag{9}$$

and for thermoelastic generation,

$$U_r(r,\nu,\omega) = \frac{j\nu^2 F_0 a}{\omega(c_{11}-c_{12})D_\nu} \frac{e^{-\alpha^2\nu^2}}{(1+j\omega\tau)^2} \times \left\{ (1-B_T) B_L \frac{J'_\nu(k_L r)}{J'_\nu(k_L a)} + \left(\nu^2 - \frac{k_T^2 a^2}{2} - B_L \right) \frac{a}{r} \frac{J_\nu(k_T r)}{J_\nu(k_T a)} \right\} \times \sum_{n=-\infty}^{+\infty} e^{j\nu 2n\pi},$$

$$U_\theta(r,\nu,\omega) = \frac{\nu F_0 a}{\omega(c_{11}-c_{12})D_\nu} \frac{e^{-\alpha^2\nu^2}}{(1+j\omega\tau)^2} \times \left\{ \nu^2 (1-B_T) \frac{a}{r} \frac{J_\nu(k_L r)}{J_\nu(k_L a)} + \left(\nu^2 - \frac{k_T^2 a^2}{2} - B_L \right) B_T \frac{J'_\nu(k_T r)}{J'_\nu(k_T a)} \right\} \times \sum_{n=-\infty}^{+\infty} e^{j\nu 2n\pi}, \tag{10}$$

where

$$\begin{aligned} D_\nu &= (\nu^2 - k_T^2 a^2/2)^2 - \nu^2 + k_T^2 a^2 (B_L + B_T)/2 \\ &\quad + (1-\nu^2) B_L B_T, \\ B_L &= k_L a J'_\nu(k_L a)/J_\nu(k_L a), \\ B_T &= k_T a J'_\nu(k_T a)/J_\nu(k_T a). \end{aligned} \tag{11}$$

Note that in Eqs. (7)–(9), $k_L = \omega\sqrt{\rho/c_{11}}$ and $k_T = \omega\sqrt{2\rho/(c_{11}-c_{12})}$ are the scalar wave vector of the longitudinal and transverse waves, respectively. Additionally, $\mathrm{sinc}(\nu\alpha) = \sin(\nu\alpha)/(\nu\alpha)$ is the sinc function, and $J'_\nu(x)$ is the derivative of the Bessel function $J_\nu(x)$.

Now, let us focus on the calculation of the integral in Eq. (8). When dealing with an elastic material, the integrand shows discontinuities for particular k_θ values. They correspond to poles associated with the zeros of the dispersion equation,

$$D_\nu = 0, \tag{12}$$

that describe the cylindrical Rayleigh waves[2] and Whispering Gallery waves.[3] The integration thus appears to be not consistent with the Fourier transformation. A suited numerical integration method should, therefore, be applied. For each value of the angular frequency ω, the integral on the real axis of the variable k_θ is calculated by means of the method suggested by Weaver *et al.*[21] In this scheme, the Fourier transform is generalized by replacing ω by a complex variable $\omega - j\delta$ with a small, constant, and imaginary part δ. With this change of variable, Eq. (8) becomes

$$u_i(r,\theta,t) = \frac{e^{\delta t}}{4\pi^2} \int \int_{-\infty}^{+\infty} U_i(r,\nu,\omega - j\delta) \times e^{-j(\nu\theta - \omega t)} d\nu \, d\omega. \tag{13}$$

The benefit of this method is twofold: (i) it preserves the application of the fast Fourier transform algorithms for the final inversion, and (ii) the integrand is a nonsingular function that may now be integrated numerically. To perform the numerical integration, the value $\delta = 0.01$ rad.μs^{-1} has been chosen for the auxiliary parameter in the following numerical calculations.

IV. EXPERIMENTAL VALIDATION

Using the inverse scheme described in Sec. III, the normal component of the displacement can be calculated for either generation at the surface of various cylinders. The calculated normal displacements are compared to the experimental signals for two aluminum cylinders of radius 4.99 and 2.06 mm. A Nd:YAG laser is used for ultrasonic wave generation in either the ablation or thermoelastic regime. The pulse duration is 20 ns and infrared light emission is obtained at 1064 nm with a maximum burst energy output of 340 mJ. The collimated optical beam is focused by means of a cylindrical lens (the focus length is 150 mm). The line length and width are about 4 cm and 0.1 mm, respectively. Using an optical heterodyne probe with a power output of 100 mW and with a sensitivity[5] of 10^{-14} m.Hz$^{-1/2}$, the normal displacement is measured at the surface. See Ref. 22 for the detail experimental setup. In this paper, the observation angle is the difference between angular coordinates of the line source and point receiver in the cylindrical reference frame.

The experimental and calculated normal displacements generated by a laser line source of 20 ns duration and 0.1 mm beamwidth under ablation generation ($a = 4.99$ mm) and thermoelastic generation ($a = 2.06$ mm) are shown in Fig. 2 and Fig. 3, respectively. The observation angle is 180°. The aluminum density considered for calculations is $\rho = 2690$ Kg.m^{-3}, and the stiffness coefficients are $c_{11}^{\mathrm{ref}} = 111.3$ GPa and $c_{12}^{\mathrm{ref}} = 59.1$ GPa.[23] The calculated wave forms have been scaled vertically by a constant corresponding to the source strength to bring the amplitudes of the two signals into the same scale. In this paper, all the time scales in the figures are dimensionless variables obtained by dividing time by a factor t_L, the arrival time of direct longitudinal wave ($t_L = 2a/V_L$, where V_L is the velocity of longitudinal waves in the studied cylinder). This dimensionless time favors the comparison, since the time scale remains unchanged for the same material with a different radius.

As shown in Figs. 2–3, the calculated and experimental wave forms are in very good agreement for both generations. The time, shape, and relative amplitude of each arrival are identical. Especially, the arrivals of the first (R_1) and the second (R_2) roundtrip of the cylindrical Rayleigh waves and their dispersive behavior (the component of the low-frequency part travels relatively fast) are clearly observed in both wave forms. The arrival of the third (R_3) roundtrip cylindrical Rayleigh wave is also calculated and measured in the thermoelastic generation. It is clear that such a cylindrical Rayleigh wave has the similar shape and dispersive property as the spherical Rayleigh wave studied by Royer *et al.*[5] The experimental and calculated direct longitudinal wave (L) and the reflected transverse wave (TT) are observed under the ablation generation, whereas they are not observable under the thermoelastic generation. This phenomenon can be explained by the different directivities of the two generation.[4] Moreover, this difference of the directivity between ablation and thermoelastic generation can also explain the relative amplitude difference of the reflected longitudinal waves (LL)

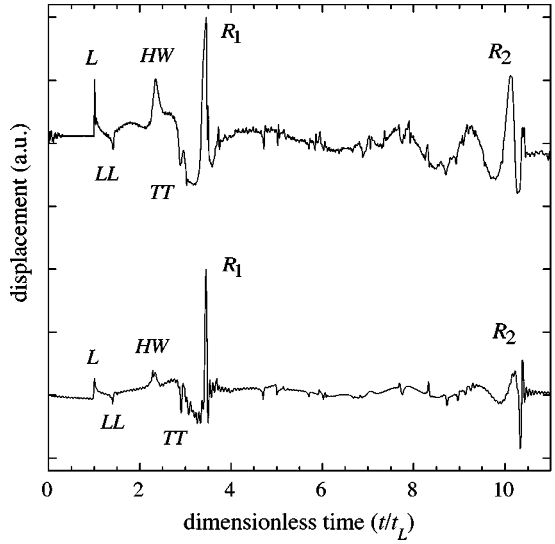

FIG. 2. Experimental (top) and calculated (below) normal displacements generated by a laser line pulse of 20 ns time duration and 0.1 mm beamwidth under the ablation regime at an observation angle of 180° for an aluminum cylinder of 4.99 mm radius.

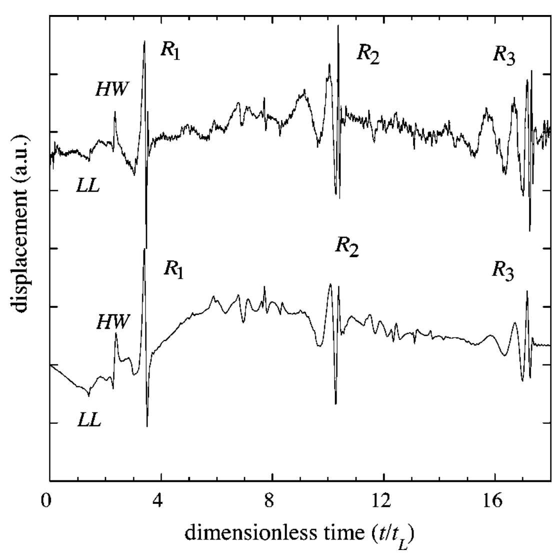

FIG. 3. Experimental (top) and calculated (below) normal displacements generated by a laser line pulse of 20 ns time duration and 0.1 mm beamwidth under the thermoelastic regime at an observation angle of 180° for an aluminum cylinder of 2.06 mm radius.

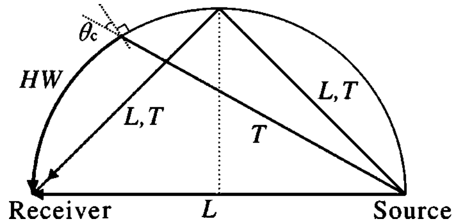

FIG. 4. Ray trajectories of *L*, *LL*, *TT*, and *HW* waves observed in Figs. 2–3. Here θ_c is the critical angle for aluminum rods.

and the head waves (*HW*) that are observed for both regimes. The ray trajectories of *L*, *LL*, *TT*, and *HW* waves are shown in Fig. 4. Following arrivals (not marked in Figs. 2–3) with small amplitude are bulk wave modes resulting from the multiple reflections of the longitudinal and transverse waves within the cylinder.[8] A comparison of the relative arrival times and amplitudes of these bulk waves emphasize the very good agreement between experiment and theory. Additionally, this comparison validates a more general calculation scheme than that already published,[10] since the time duration and beamwidth are taken into account here, whereas the Green's function was considered previously.

V. EFFECTS OF TIME DURATION AND BEAMWIDTH

Analyzing the effects of the source beamwidth and the time duration of the laser is necessary for the application purpose. As presented in Sec. IV, cylindrical Rayleigh waves, various longitudinal and transverse bulk waves are clearly observable in the experimental wave forms for two aluminum cylinders. If further attempting to recover elastic constants by measuring the time arrivals of selected waves, one possibly raises such a question as whether these waves are still observable for a very small cylinder. To respond this question, one must study their effects on these wave modes. In other words, one must understand how the shape and relative amplitude of a selected wave mode change along with the size of the cylinder.

For such an analysis, numerical simulation instead of experiment is preferred. The simulation can be performed on the present model. Even though these effects can be studied by experimenting on cylinders with radii covering a wide range, simulating is relatively direct, complete, and clear. The numerical simulations are carried in two folds: (i) study the effect of the source time duration by varying the radius of the cylinder while excluding the effect of the source beamwidth; and (ii) study the effect of the source beamwidth by varying the radius of the cylinder while excluding the effect of the source time duration.

A. Source time duration

First let us analyze the effect of the source time duration. Since a laser pulse generally has a fixed time duration τ, this effect is analyzed at different τ/t_L ratios by varying the radius of the cylinder. The source beamwidth is assumed to be zero to exclude its effect. The low limit of τ/t_L is zero, and its upper limit is estimated as two if supposing no bulk wave is observed when half the equivalent wavelength $\lambda_\tau = \tau V_L$ is greater than $2a$, the diameter of the cylinder. Applying the numerical inverse scheme described in Sec. III, normal displacements at an observation angle of 180° for aluminum cylinders under either ablation or thermoelastic generation are calculated for τ/t_L ratios of 0, 0.02, 0.1, 0.2, 0.4, 0.8, and 2. Results are shown in Figs. 5–6, where the wave forms are vertically scaled to obtain the same maximum amplitude for each of them. To fix ideas, the ratio between maxima obtained for τ/t_L equal 0 and 2, is 26 and 2 for Fig. 5 and Fig. 6, respectively. Under both regimes, the surface and various bulk waves are losing more of their relatively high-frequency components, and their amplitudes are becoming flatter until they have completely disappeared, when ratios τ/t_L increase from 0 to 2. Since the time duration of the pulse acts as a low-pass filtering with its bandwidth inversely proportional to τ, it cuts off more of their relatively high-frequency parts

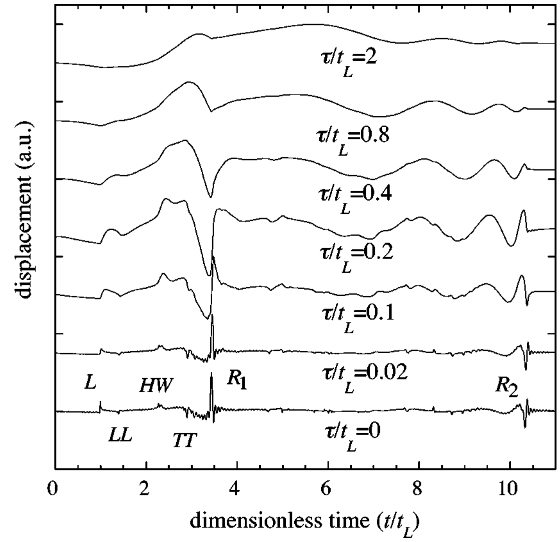

FIG. 5. Calculated normal displacements at an observation angle of 180° for aluminum cylinders under the ablation generation for different ratios of the source time duration τ over t_L the arrival time of the direct longitudinal wave.

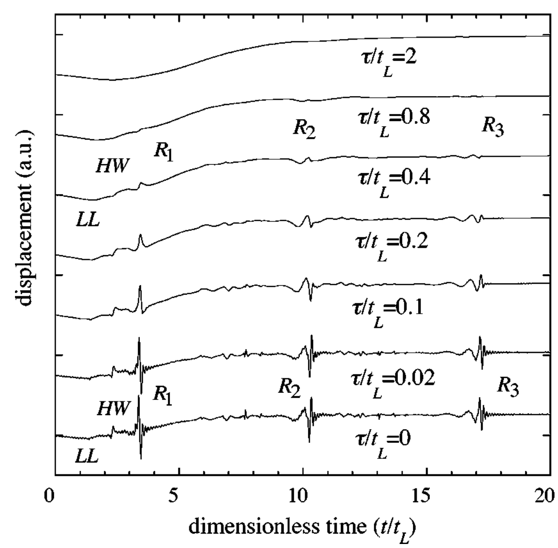

FIG. 6. Calculated normal displacements at an observation angle of 180° for aluminum cylinders under the thermoelastic generation for different ratios of the source time duration τ over t_L the arrival time of the direct longitudinal wave.

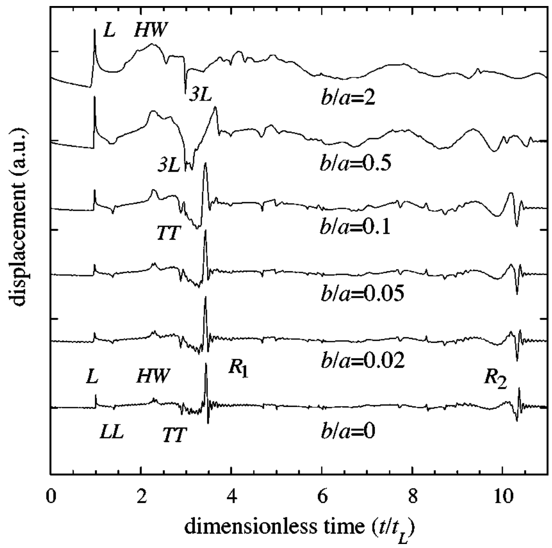

FIG. 7. Calculated normal displacements at an observation angle of 180° for aluminum cylinders under the ablation generation for different ratios of the source beamwith b over the cylinder radius a.

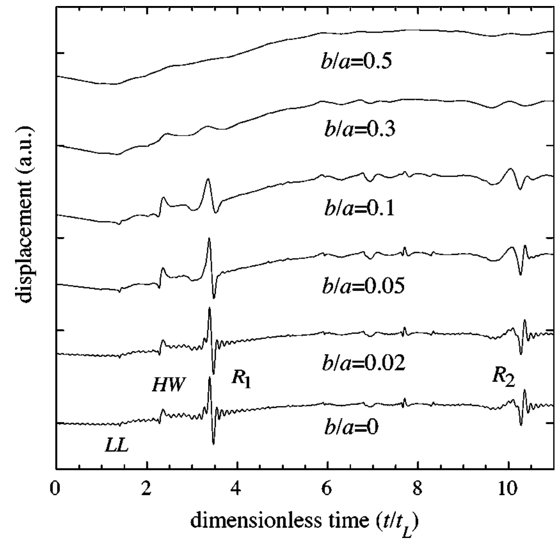

FIG. 8. Calculated normal displacements at an observation angle of 180° for aluminum cylinders under the thermoelastic generation for different ratios of the source beamwith b over the cylinder radius a.

when τ increases. Owing to this filtering, two successive echoes cannot be distinguished if the delay between their arrivals is less than the time duration. Considering the direct longitudinal L and once reflected longitudinal LL (the time arrival is $t_{LL}=\sqrt{2}t_L$) waves, it comes that they cannot be separated if τ/t_L is greater than 0.4. This is in agreement with the evolution of the wave forms plotted in Figs. 5–6. In other words, if time arrivals are required for nondestructive evaluation (NDE) purposes, cylinders with a radius less than $1.25\tau V_L$ should not be chosen. For a laser source of 20 ns time duration, this radius limit is 0.16 mm for an aluminum rod.

B. Source beamwidth

Now let us analyze the effect of the source beamwidth. As a finely focused laser generally has a certain beamwidth b, this effect is analyzed at different b/a ratios by varying the radius of the cylinder. The low limit of b/a ratio is zero, and its upper limit is two. Here the source time duration is assumed to be zero to exclude its influence. As shown in Fig. 7 and Fig. 8, normal displacements at an observation angle of 180° for aluminum cylinders are calculated for b/a ratios of 0, 0.02, 0.05, 0.1, 0.5, and 2 under ablation generation and of 0, 0.02, 0.05, 0.1, 0.3, and 0.5 under thermoelastic generation. The wave forms are also vertically scaled. The ratio between maxima obtained for b/a equal 0 and 2 is 9 for Fig. 7, and this ratio for b/a equal 0 and 0.5 is 3 for Fig. 8. In the ablation generation, Fig. 7, the amplitude of the direct longitudinal wave (L) and that of the directly reflected wave ($3L$) propagating back and forth along the cylinder diameter increase when b/a changes from 0 to 2, and no filtering occurs. Relative amplitudes of other bulk waves and surface waves flatten, until they completely disappear. However, HW arrivals are still observable. Increasing the source width acts as a low-pass filtering in the ν domain. As detailed in Ref. 24, this filtering changes the source directivity, and enlarging the source size favors the generation of longitudinal waves in a direction normal to the interface for this generation. In the thermoelastic generation, Fig. 8, since the source directivities of two generations are different, LL waves are observable whereas L waves are no more distinguishable. Wave forms are therefore more affected by increasing source size in this generation than in the ablation generation. Consequently, bulk LL and HW waves are not observable when b/a reaches 0.5, but they are slightly affected by the source directivity for ratio b/a up to 0.3. For a laser source of 0.1 mm beamwidth, the cylinder radius limit is about 0.3 mm for NDE purposes.

When experimental signals are considered, both effects should be considered simultaneously. Therefore, for NDE application using bulk waves, a radius of 0.3 mm appears as a minimum limit for the sample size with our experimental devices.

VI. APPLICATION TO THE MEASUREMENT OF ELASTIC CONSTANTS

As an inverse problem, it is generally considered to recover the elastic constants by the time arrivals of acoustic waves detected through the laser ultrasonic system. As described in Sec. II, two independent elastic constants, c_{11} and c_{12}, are related to the isotropic plane of a transversely isotropic cylinder, and they link with the longitudinal and transverse wave velocities V_L and V_T by the following equation:

$$c_{11}=\rho V_L^2$$

$$c_{12}=\rho(V_L^2-2V_T^2). \tag{14}$$

Since the mass density ρ and radius a of the tested cylinder can be easily measured, these two velocities V_L and V_T should be obtained at the same time for the measurement. Now let us determine how to measure the two velocities under either ablation or thermoelastic generation.

First let us look at the experimental waveform under ablation generation in Fig. 2. The longitudinal wave velocity V_L can be determined by measuring the arrival time of the direct longitudinal wave (L), or the reflected longitudinal

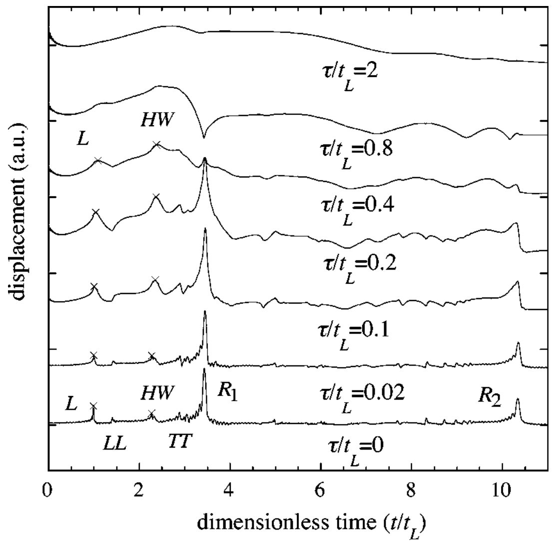

FIG. 9. Moduli of the analytic signals associated to the calculated normal displacements in Fig. 5. Crosses show the positions of the maximum moduli considered for the wave arrivals.

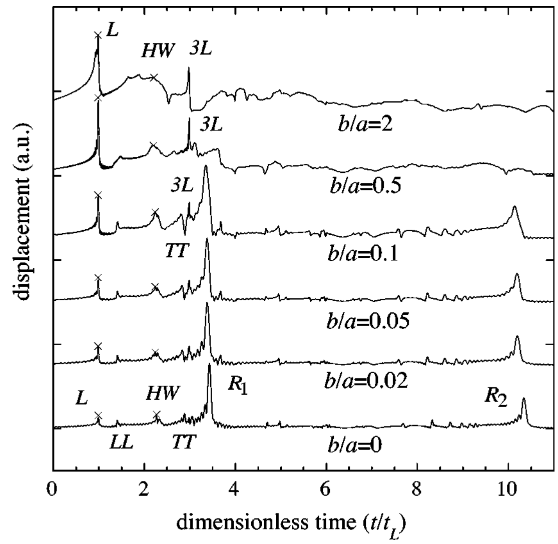

FIG. 10. Moduli of the analytic signals associated to the calculated normal displacements in Fig. 7. Crosses show the positions of the maximum moduli considered for the wave arrivals.

wave (LL). The transverse wave velocity V_T can be determined by measuring the arrival time of the reflected transverse wave (TT), or the head wave (HW) after V_L was determined. The arrival time of head wave t_{HW} links with V_L and V_T by the formulas $t_{HW}=t_L(\beta+\cot\beta)$ and $\beta=\sin^{-1}(V_T/V_L)$. Owing to their relative amplitudes, L and HW waves are chosen for the measurement. Although the cylinder Rayleigh wave has a high amplitude, it is not considered here since it is dispersive.[5] The following bulk waves are also not considered as they have relative low amplitude. Then let us look at the experimental wave form under thermoelastic generation in Fig. 3. The longitudinal wave velocity V_L can be determined by measuring the arrival time of the reflected longitudinal wave (LL). The transverse wave velocity V_T can be determined by measuring the arrival time of the head wave HW after V_L was determined. The cylinder Rayleigh wave is also not considered for the same reason as for the ablation generation. Following bulk waves, having undergone several reflections with or without mode conversion at the cylinder interface, could also be used since their amplitude can be high. However, they are not considered here since recovering of their exact paths is not a trivial matter. The above measurement schemes of both regimes only hold true for experiments at an observation angle 180°. If another observation angle is chosen as presented in the experimental setup of Clorennec and Royer,[15] a different scheme can be found after acoustic waves are identified by the published model[10] or the model presented in Sec. II.

It is also direct and complete to analyze the effects of source time duration and beamwidth on the measurement by processing the calculated wave forms. First let us look at the effect of time duration under ablation generation. In order to determine the arrival time of selected waves in the calculated wave forms in Fig. 5 of the last section, a signal processing published by one of the authors[25] is applied to locate the wave arrivals. The moduli of the analytic signals[25] associated to wave forms in Fig. 5 are shown in Fig. 9. Numerical interpolation is further adopted to precise the maximum positions corresponding to the arrivals of L and HW waves. These positions are marked with crosses in Fig. 9. The two elastic constants are calculated from t_L the arrival time of the L wave and t_{HW} the arrival time of the HW wave, and they are compared to the reference values in Sec. IV used to calculate the wave forms. As reported in Table I, their deviations increase as τ/t_L turns to 0.4, and it is difficult to determine the elastic constants when τ/t_L is greater than 0.4. Then let us look at the effect of beamwidth under ablation generation. As shown in Fig. 10, applying the same signal processing yields the moduli of the analytic signals associated to wave forms in Fig. 7. The determined elastic constants are

TABLE I. The deviations of the elastic constants determined from the calculated wave forms under ablation (Fig. 5) and thermoelastic (Fig. 6) regimes for various τ/t_L ratios.

	Ablation regime		Thermoelastic regime	
t/t_L	$(c_{11}-c_{11}^{\mathrm{ref}})/c_{11}^{\mathrm{ref}}$	$(c_{12}-c_{12}^{\mathrm{ref}})/c_{12}^{\mathrm{ref}}$	$(c_{11}-c_{11}^{\mathrm{ref}})/c_{11}^{\mathrm{ref}}$	$(c_{12}-c_{12}^{\mathrm{ref}})/c_{12}^{\mathrm{ref}}$
0	0.3%	−2.0%	−0.9%	−1.5%
0.02	0.5%	−5.2%	1.4%	1.5%
0.1	−1.3%	−6.9%	−6.7%	−8.4%
0.2	−7.9%	−13.1%	−9.6%	−13.1%
0.4	−16.0%	−20.8%	−9.7%	−13.5%

TABLE II. The deviations of the elastic constants determined from the calculated wave forms under ablation (Fig. 7) and thermoelastic (Fig. 8) regimes for various b/a ratios.

	Ablation regime		Thermoelastic regime	
b/a	$(c_{11}-c_{11}^{\mathrm{ref}})/c_{11}^{\mathrm{ref}}$	$(c_{12}-c_{12}^{\mathrm{ref}})/c_{12}^{\mathrm{ref}}$	$(c_{11}-c_{11}^{\mathrm{ref}})/c_{11}^{\mathrm{ref}}$	$(c_{12}-c_{12}^{\mathrm{ref}})/c_{12}^{\mathrm{ref}}$
0	0.3%	−2.0%	−0.9%	−1.5%
0.02	3.5%	0.8%	1.5%	1.7%
0.05	3.5%	0.7%	1.5%	1.8%
0.1	3.5%	0.6%	1.3%	1.5%
0.3	⋯	⋯	1.6%	−4.9%
0.5	3.5%	−3.9%	⋯	⋯
2	3.3%	−2.6%	⋯	⋯

TABLE III. Elastic constants measured for aluminum rods of various radii.

Regimes	a (mm)	b/a	τ/t_L	c_{11} (GPa)	c_{12} (GPa)
Ablation (Fig. 2)	4.99	0.02	0.013	110	61
Thermoelastic (Fig. 3)	2.06	0.05	0.032	111	58
Thermoelastic	1.00	0.1	0.064	110	61
Thermoelastic	0.50	0.2	0.128	113	62

also compared to the reference values. As listed in Table II, their deviations are of the same level when b/a turns to 2. It could be concluded that the laser beamwidth does not affect the elastic constant measurement for ablation generation. As also reported in Table I, the effect of the source time duration under thermoelastic generation is of the same order of magnitude as under ablation generation, and similar comments can be suggested. But the effect of the source beamwidth under thermoelastic generation is a little different from that under ablation generation. As also listed in Table II, the bulk waves are not measurable when b/a reaches 0.5, because the directivities of two regimes are different.[4]

Finally, let us carry the same signal processing on experimental signals under either regime shown in Figs. 2–3. Additionally, two aluminum rods with radii of 1.00 and 0.50 mm are further chosen for the measurement under a thermoelastic regime. The measured elastic constants are reported in Table III. These values are very close to that in the reference.[23] The deviations for the measured elastic constant c_{11}, estimated from the simulation results in Tables I and II, are 4%, 6%, 7%, and 10% for the aluminum rods of radii 4.99, 2.06, 1.00, and 0.50 mm, respectively. The corresponding deviations for another elastic constant c_{12} are estimated to be 5%, 7%, 8%, and 13%. Here, the relatively large deviation for a pair of τ/t_L and b/a ratios is assumed to take into account of both effects of the source time duration and beamwidth. These deviations remain low, even for the cylinder whose radius is close to the minimum limit estimated in Sec. V. Actually, these deviations will be much smaller if the measured elastic constants are compared to the reference values.

It can be concluded that the waves are correctly identified, and that the method used to measure the time arrivals is suitable for such a purpose of elastic constants recovery.

VII. CONCLUSION

A theoretical model has been presented to predict the acoustic field generated by a laser line pulse extended in the beamwidth and time duration under either the ablation or thermoelastic regime at any point of a homogeneous and transversely isotropic cylinder. Experimental and theoretical normal displacements under either regime were obtained and compared for aluminum cylinders. Very good agreements are observed in the time, shape and relative amplitude (i) of the cylindrical Rayleigh waves with different roundtrips, and (ii) of the various longitudinal and transverse bulk waves propagating through the cylinder or reflected at the free circular surface.

The effects of the source beamwidth and time duration have been analyzed by varying the radius of the cylinder. The source time duration under either regime acts as a low-pass filtering with its bandwidth inversely proportional to its width in time. The source beamwidth affects the directivities of both longitudinal and transverse waves for either regime. Enlarging the source size favors the generation of longitudinal waves in a direction normal to the interface for ablation generation. For NDE applications using bulk waves, a radius of 0.3 mm appears as a minimum limit for the sample size using a laser of 0.1 mm beamwidth and 20 ns time duration.

To recover the elastic constants, the velocity of the longitudinal wave could be first determined by measuring the arrival time of the direct longitudinal wave for ablation generation or that of the reflected longitudinal wave for thermoelastic generation, and then the velocity of the transverse wave could be determined by measuring the arrival time of the head wave for either generation. The source beamwidth slightly affects the elastic constant measurement, whereas the measurement error enlarges as the source time duration increases. Such a measurement scheme including the signal processing is further justified by results on experimental wave forms detected on aluminum rods under ablation and thermoelastic generations.

ACKNOWLEDGMENTS

This work was done at the Laboratoire de Mécanique Physique, Université Bordeaux 1. One of the authors (Y. P.) was supported by the National Center for Scientific Research of France (CNRS) and the China Scholarship Council.

[1] K. Sezawa, "Dispersion of elastic waves propagated on the surface of stratified bodies and on curved surfaces" Bull. Earthquake Res. Inst., Univ. Tokyo **3**, 1–18 (1927).
[2] A. Viktorov, *Rayleigh and Lamb Waves* (Plenum, New York, 1967).
[3] H. Uberall, *Physical Acoustics* (Academic, New York, 1973), Vol. 10, p. 1–60.
[4] C. B. Scruby and L. E. Drain, *Laser Ultrasonics: Techniques and Applications* (Adam Hilger, New York, 1990).
[5] D. Royer, E. Dieulesaint, X. Jia, and Y. Shui, "Optical generation and detection of surface acoustic waves on a sphere," Appl. Phys. Lett. **52**, 706–708 (1988).
[6] S. Ishikawa, H. Cho, Y. Tsukahara, N. Nakaso, and K. Yamanaka, "Analysis of spurious bulk waves in ball surface wave device," Ultrasonics **41**, 1–8 (2003).
[7] M. Qian and X. Wu, "Studies of cylindrical Rayleigh waves with laser ultrasonics," Prog. Nat. Sci. **11**, s258–s264 (2001).
[8] D. Clorennec and D. Royer, "Analysis of surface acoustic wave propagation on a cylinder using laser ultrasonics," Appl. Phys. Lett. **82**, 4608–4610 (2003).
[9] X. Wu and M. Qian, "Simulation of the finite element method on wave propagation in cylinders," Prog. Nat. Sci. **11**, s265–s268 (2001).
[10] Y. Pan, C. Rossignol, and B. Audoin, "Acoustic waves generated by a laser line pulse in a transversely isotropic cylinder," Appl. Phys. Lett. **82**, 4379–4381 (2003).
[11] F. Honarvar and A. N. Sinclair, "Nondestructive evaluation of cylindrical components by resonance acoustic spectroscopy," Ultrasonics **36**, 845–854 (1998).

[12] Y. A. Burenkov and S. P. Nikanorov, ''Elastic properties and binding forces in crystals with diamond and sphalerite lattices,'' Sov. Phys. Solid State **26**, 1940–1944 (1984).
[13] C. P. Lusher and W. N. Hardy, ''Axisymmetric free vibrations of a transversely isotropic finite cylindrical rod,'' J. Appl. Mech. **55**, 855–862 (1988).
[14] M. Qian, M. Duquennoy, M. Ouatouh, F. Jenot, and M. Ourak, ''Laser ultrasonic characterization of surface residual stresses in steel rods,'' Rev. Prog. Quant. Nondestr. Eval. **20**, 1487–1493 (2001).
[15] D. Clorennec, D. Royer, and H. Walaszek, ''Nondestructive evaluation of cylindrical parts using laser ultrasonics,'' Ultrasonics **40**, 783–789 (2002).
[16] A. Rahman and F. Ahmad, ''Representation of the displacement in terms of scalar functions for use in transversely isotropic materials,'' J. Acoust. Soc. Am. **104**, 3675–3676 (1998).
[17] L. R. F. Rose, ''Point-source representation for laser-generated ultrasound,'' J. Acoust. Soc. Am. **75**, 723–732 (1984).
[18] D. A. Hutchins, *Physical Acoustics* (Academic, New York, 1988), Vol. 18, pp. 21–123.
[19] Y. H. Berthelot and I. J. Busch-Vishniac, ''Thermoacoustic radiation of sound by a moving laser source'' J. Acoust. Soc. Am. **81**, 317–327 (1987).
[20] C. B. Scruby, R. J. Dewhurst, D. A. Hutchins, and S. B. Palmer, ''Quantitative studies of thermally generated elastic waves in laser-irradiated metals,'' J. Appl. Phys. **51**, 6210–6216 (1980).
[21] R. L. Weaver, W. Sachse, and K. Y. Kim, ''Transient elastic waves in a transversely isotropic plate,'' J. Appl. Mech. **63**, 337–346 (1996).
[22] F. Reverdy and B. Audoin, ''Elastic constants determination of anisotropic materials from phase velocities of acoustic waves generated and detected by lasers,'' J. Acoust. Soc. Am. **109**, 1965–1972 (2001).
[23] O. L. Anderson, *Physical Acoustics* (Academic, New York, 1965), Vol. 3, pp. 43–95.
[24] J. D. Aussel, A. Le Brun, and J. C. Baboux, ''Generating acoustic waves by laser: Theoretical and experimental study of the emission source,'' Ultrasonics **26**, 245–255 (1988).
[25] B. Audoin, C. Bescond, and M. Deschamps, ''Measurement of stiffness coefficients of anisotropic materials from pointlike generation and detection of acoustic waves,'' J. Appl. Phys. **80**, 3760–3771 (1996).